Design Methodology of a Brushless IPM Machine for a Zero-Speed Injection Based Sensorless Control

J.Godbehere, R.Wrobel, D.Drury and P.H.Mellor
Electrical Energy Management Group
University of Bristol,
Bristol, UK.
E-mail: jg7560@bristol.ac.uk

Abstract — **In this paper a design approach for a sensorless controlled, brushless, interior permanent magnet machine is attained. An initial study based on established electrical machine formulas provides the machine's basic geometrical sizing. The next design stage combines a particle swarm optimisation (PSO) search routine with a magneto-static finite element (FE) solver to provide a more in depth optimisation. The optimisation system has been formulated to derive alternative machine design variants, subject to the design constraints, in a computationally efficient manner using as few FE simulations as required. Moreover a parallel computing approach has been used for the most computationally intensive processes. The optimisation system objective function aims to find a solution satisfying all the machine's design requirements including the torque-speed envelope and compatibility with the high-frequency injection based sensorless operation, whilst minimising the machine weight.**

A holistic approach is presented where a complete machine, including the stator and rotor sub-assemblies are designed accounting for all the required performance measures under the high-frequency injection based sensorless operation. The efficacy of the new approach has been demonstrated on a design case study with consecutive design stages discussed in detail. Also, the paper provides conceptual information regarding practical implementation of the proposed optimisation system together with an insight into the definition of the objective function and its influence on the design solutions. Furthermore, the calculated results from the optimisation system have been compared with direct FE predictions for the design exemplar showing good correlation.

Keywords—Design Methodology, Sensorless Control, Interior Permanent Magnet (IPM), Particle Swarm Optimisation.

I. INTRODUCTION

Sensorless control of machines offers the benefits of reduced system cost and improved reliability by eliminating the need for a shaft mounted position sensor. A typical implementation of sensorless operation across the full operational range combines a back EMF flux estimator for mid to high speed ranges with high-frequency signal injection techniques for zero and low speed ranges [1].

Machine design for sensorless control involves the requirements of the sensorless control algorithm to be embedded within the design process. The aim is to tailor the design to boost the electromagnetic characteristic that are critical to the success of the sensorless algorithm, without compromising other more general performance requirements. The idea being that a machine with desirable sensorless performance will present a reliable rotor position signature across the full operating torque range, allowing the use of simpler control schemes which do not require tuning to a specific machine or complicated error correction routines [2].

Sensorless operation at zero and low operating speeds requires an electromagnetic signature to be incorporated into the machine design which can be detected to yield positional information. In the case of a PM machine the most common way of achieving this is to use a salient rotor design where the quadrature axis inductance is greater than the direct axis inductance. Since the rotor position signal is dependent on a difference between the L_d and L_q inductances it is essential that the saliency ratio (L_q/L_d) is measurable across the full range of torque [3]. In a machine designed to operate at a high flux density the values of inductance will change due to saturation and cause the magnitude of the saliency to decrease, in some cases even reverse. In addition slotting effects may alter these values further. Therefore the saliency characteristic tends to be a function of both load and rotor position.

Secondary magnetic effects can introduce a dependent error in the rotor position. This is mainly due to cross coupling between the direct (d) and quadrature (q) axis inductances [4], [5]. The error can be quite significant and if left uncompensated may result in a significant performance degradation. Minimising this error is also an important criteria. The ideal machine for a sensorless control scheme would have a high absolute value of saliency over the full range of torque, low angular error and little variation to either over the full rotation of the machine.

Published work in this field has mainly focused on the design of the rotor, including choice of rotor topology and the use of optimisation routines [6–10]. Other papers have shown that the type of winding configuration (i.e. concentrated or distributed) [11] and the slot shape [12] can have a large effect on the sensorless capability of a machine. However there is little published work on how to design a complete machine for sensorless control in a holistic manner. Often design methodologies are presented where only the sensorless aspect of the rotor design is considered and the stator is left unchanged.

Designing a rotor with a high saliency may not be sufficient to guarantee good sensorless performance. The sensorless performance can be strongly influenced by slotting effects, the winding configuration and the level of flux density in the stator iron. Therefore optimum performance can only be achieved by designing the two components simultaneously.

The basic saliency detection process based on signal injection can be replicated in finite element analysis (FEA) to a high level of accuracy [10]. As the degree of saliency will vary with both load and rotor position direct FE analysis of a machine would require many simulations. This is computationally prohibitive in the context of a design optimisation. This issue is addressed in the paper through a formulation which incorporates numerical and analytical methods.

The proposed methodology has been demonstrated on an IPM machine design, as this topology offers an intrinsically higher saliency compared to other rotor types. [13].

II. Overwiew of initial Machine requirements

The target specification is a low speed, high torque motor. The application requirement is a transient duty cycle with only a short period of operation at full torque. The space envelope available does not restrict the overall diameter or length of the machine. However it is desirable for the final solution be as compact and as low weight as possible. The motor specification is summarised in Table I.

TABLE I. Machine operating envelope specifications

Peak Power (kW)	Peak Torque (Nm)	Maximum Speed (RPM)	DC link voltage (V)
1.5	47	420	28

It is desirable to use a high number of poles due to the low speed and high torque requirement of the machine. To reduce the complexity of the rotor structure in light of this, a single layer IPM rotor topology is chosen for the basis of the work [4].

A. Initial Design Assumptions

The initial design assumptions have been made based on requirements regarding the machine's intended operating duty cycle and cooling regime. From these target values for the magnetic loading, electrical loading and winding current density are defined respectively:

$B_1 = 0.8$ T, $Q_{rms} = 100{,}000$ A/m, $J_{rms} = 27$ A_{rms}/mm^2

B. Basis Of The Sensorless Control Algorithm

A three-phase sinusoidal injection signal is used as the base for the sensorless control strategy. In such a scheme a high frequency voltage is injected onto the stator winding. The high frequency current variation due to this injected signal provides the rotor position information when a magnetic saliency is present. Represented in the αβ reference frame the injected voltage is:

$$v_{\alpha\beta} = V_i \begin{pmatrix} -\cos(\omega_i t) \\ \sin(\omega_i t) \end{pmatrix} \quad (1)$$

Considering the dq-model for a PM machine:

$$v_{dq} = \begin{pmatrix} R_s + pL_d & \omega_r L_q \\ \omega_r L_d & R_s + pL_q \end{pmatrix} i_{dq} + \begin{pmatrix} 0 \\ \psi_m \omega_r \end{pmatrix} \quad (2)$$

If the angular frequency of the injected signal, ω_i, is sufficiently high then only the inductance of the stator windings need to be considered. If the machine is operating at zero or a low speed then the rotor rotational speed is also negligible compared to the injected voltage. The machine can therefore be assumed to be stationary and so the machine model can be approximated in the αβ reference frame as:

$$v_{\alpha\beta} \approx j\omega_i L_{\alpha\beta} i_{\alpha\beta} \quad (3)$$

Evaluating (3) with the high frequency voltage signal shown in (1), it can be shown that the resulting high frequency current is:

$$i_{\alpha\beta} = I_1 \begin{pmatrix} \cos(\omega_i t) \\ \sin(\omega_i t) \end{pmatrix} - I_2 \begin{pmatrix} \cos(2\theta_r - \omega_i t) \\ \sin(2\theta_r - \omega_i t) \end{pmatrix} \quad (4)$$

I_1 and I_2 will vary based upon the inductance of the machine and the injection signal used. The rotor position information θ_r is contained within the second term of (4). When isolated through the use of the Park transform and high-pass filters the high frequency current response is:

$$\begin{pmatrix} i_x \\ i_y \end{pmatrix} = -I_2 \begin{pmatrix} \cos(2\theta_r) \\ \sin(2\theta_r) \end{pmatrix} \quad (5)$$

The above derivation is basis of an open loop implementation of the frequency injection method. Alternative sensorless algorithms use a closed loop form of control [1] and tracking to improve the accuracy of the technique to account for effects such as torque ripple, noise and inverter commutation.

III. Design procedure

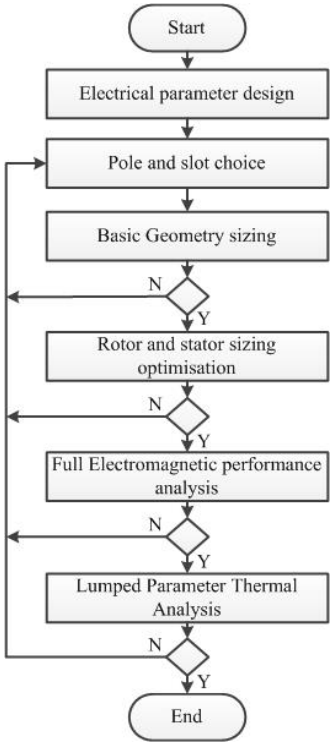

Fig. 1. Top level design methodology

The proposed design process is presented in Fig.1, and is formed of two main parts; an initial trade study and an optimisation procedure. The process is iterative as the performance of each design iteration is analysed at the end of each section. Changes are made to the machine parameters based upon these results until a satisfactory design is found.

A full electromagnetic and thermal analysis is conducted on the designs which demonstrate the best potential. This will serve to validate if they have achieved all the performance requirements of the specification, but are too computationally expensive to conduct during an optimisation procedure.

A. Analytical Trade Study

The first stage of the procedure employs an equivalent circuit based analysis to specify target values for the EMF constant and inductance. When these parameters are met by the design then the required torque and speed envelope will be electrically achievable within the constraints of the supply system.

At this initial stage the saliency ratio is fixed and ideal operation is considered. Alternative pole (p) and slot (q) combinations are investigated. These are chosen based on the value for the fundamental winding factor (K_{w1}) and the magnitude of the cogging torque. Torque ripple effects are gauged by value of the lowest-common-multiple between the pole and slot numbers. Both concentrated and distributed winding topologies have been investigated.

An estimate for the number of turns per slot (N_s) is first made and an aspect ratio is chosen. The aspect ratio is defined as the ratio of the stator bore to active length (6).

$$Aspect\ Ratio = \frac{D}{L} \tag{6}$$

The resulting stator bore and active length are sized based upon the required torque and initial assumptions for electrical loading (Q_{rms}), magnetic loading (B_1) and the winding factor (K_{w1}) (7). An estimate for the base torque must be made based upon the saliency value that is expected to be achieved in the design.

$$T_{base} = \frac{\pi}{2\sqrt{2}} D^2 L B Q_{RMS} K_{w1} \tag{7}$$

The predicted back EMF constant (K_e) can then be calculated (8). If this value is unsatisfactory compared to the target value needed to reach the operational envelope then either the number of turns per slot or aspect ratio are altered.

$$K_e = \left(N_s \frac{q}{3}\right) D L B K_{w1} \tag{8}$$

Finally the rms phase current (I_{prms}) is calculated from the electrical loading, stator bore and number of turns per slot (9).

$$Q_{rms} = \frac{6\left(N_s \frac{q}{3}\right) I_{prms}}{\pi D} \tag{9}$$

A 16 pole, 72 slot machine is chosen to demonstrate the complete design process. This was determined to be the best solution for the chosen application based upon its low cogging torque, high fundamental winding factor and high saliency due to the high number of slots. The input data for the next stage of the design procedure is shown in Table II.

TABLE II. MACHINE DESIGN CHOICES FOR OPTIMISATION

No. Poles (p)	No. Slots (q)	Stator Bore (D) (mm)	Active Length (L) (mm)	Air gap (g) (mm)	RMS phase current (I_{prms}) (A_{rms})	Turns per slot (N_s)	Slot fill factor (k_p)
16	72	111.9	37.3	0.8	61.1	4	0.5

B. Design Optimisation Procedure

The design optimisation aims to tune the design of the stator and rotor in more detail against the design objectives, whilst taking into account non-linear effects such as saturation. The optimisation must be able to accurately assess the performance of a design, be computationally efficient, find the best design possible but be constrained such that the final design is in fact feasible.

The computation time of the optimisation is dominated by the time required to run a numerical finite element (FE) simulation. As such the total execution time of the optimisation routine is determined by the number of FE simulations needed to asses each individual design.

TABLE III. VARIABLES WITHIN THE OPTIMISATION SYSTEM AND EXAMPLE RANGE

Number	Parameter	Range
1	Rotor pole arc angle	80° - 135°
2	V-pole angle	160° - 180°
3	PM thickness	1 mm - 6.8 mm
4	Bridge thickness	0.2 mm - 1.5 mm
5	Web thickness	0.5 mm - 2 mm
6	Web length	0mm - 7mm
7	Split Ratio (D / (7))	0.55 - 0.8
8	Yoke thickness	1 mm – 11 mm
9	Slot width	0.5 mm - 4 mm
10	Slot opening	0.5 mm – 4 mm
11	Tooth depth	0.5 mm - 1.5 mm

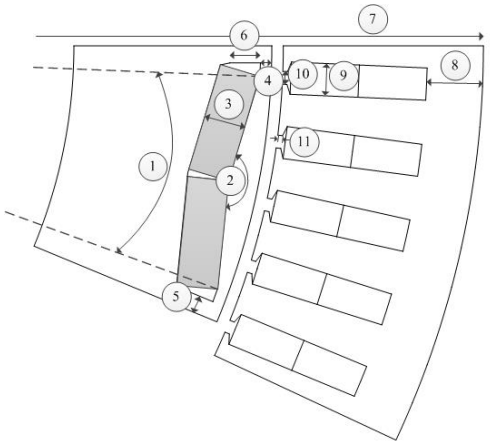

Fig. 2. Outline of V-IPM machine with labels indicating variables within optimisation

In order to minimise the number of numerical FE analyses only the most demanding operating point for the machine is considered. Full rated current is used as this is the point at which the saliency will be at its lowest due to saturation in the iron circuit. If the performance at this point is satisfactory, then it is expected to be at other, lower values of current. The same fixed rotor position is used for all the designs. A more in depth analysis to investigate the variation of the saliency with changing rotor position is performed later for the designs which demonstrate the best performance.

The parametrisation of the IPM machine and example of the assumed ranges of these parameters are included in Fig.2 and Table III. This range is applicable to the specific inputs shown in Table II and should be tailored for an individual design. The ranges are determined so that any combination of the variables within that range will generate a valid machine geometry.

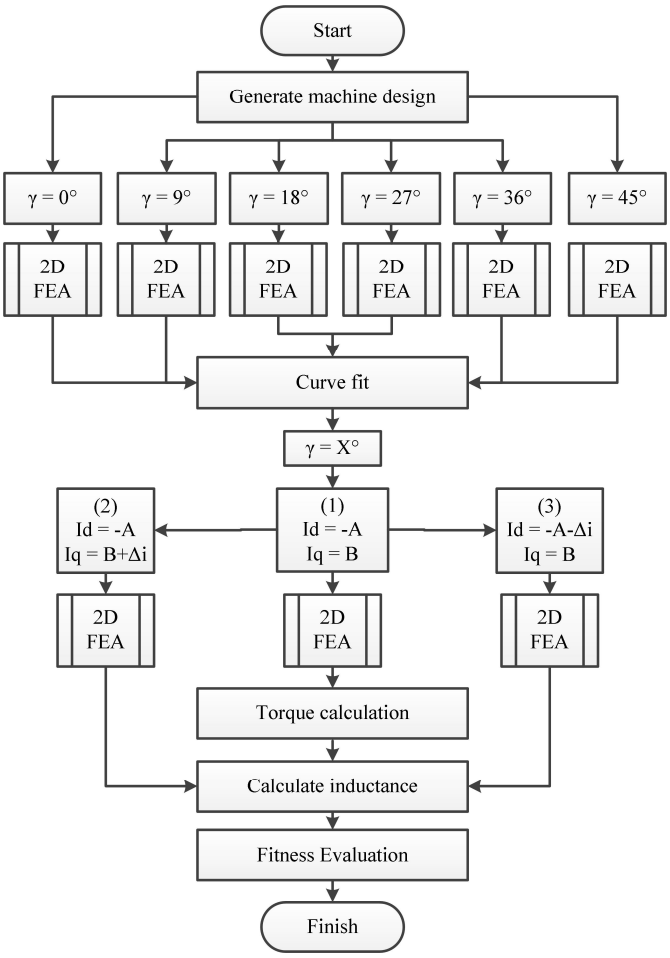

Fig. 3. Detailed FE simulation routine for a single particle in the optimisation system

Torque and inductance are the two main outputs needed to judge the performance of a machine design. A method for calculating these using only three FE simulations is described in [14]. A simulation is first conducted at rated current (labelled 1 in Fig. 3). Then two further simulations are conducted, one with a small increase in q-axis current ($\Delta i = 0.1$ A), and the other with d-axis current (labelled 2 and 3 in Fig. 4). The d and q axis inductances can be calculated from the change in flux linkage between these points, (10) and (11). In addition values catering for a magnetic cross coupling component (L_{dq} and L_{qd}) can be calculated, (12) and (13). In a later section it will be shown how these four components can be used to estimate the sensorless capability of a machine design.

Torque is estimated from the winding flux linkage obtained from each FE solution, and the current used. Calculating torque in this manner will ignore any torque ripple components, and such will be closer to the average torque value (14).

$$L_d = \frac{\partial \lambda_d}{\partial i_d} \approx \frac{\lambda_{d(3)} - \lambda_{d(1)}}{\Delta I_d} \tag{10}$$

$$L_q = \frac{\partial \lambda_q}{\partial i_q} \approx \frac{\lambda_{q(2)} - \lambda_{q(1)}}{\Delta I_q} \tag{11}$$

$$L_{dq} = \frac{\partial \lambda_d}{\partial i_q} \approx \frac{\lambda_{d(2)} - \lambda_{d(1)}}{\Delta I_q} \tag{12}$$

$$L_q = \frac{\partial \lambda_q}{\partial i_q} \approx \frac{\lambda_{q,(3)} - \lambda_{q,(1)}}{\Delta I_q} \tag{13}$$

$$T = \frac{3}{2} p\left(\lambda_{d(1)} I_q - \lambda_{q(1)} I_d\right) \tag{14}$$

The values of I_d and I_q are calculated based upon the rated rms current (I_{prms}) and the current angle (γ) as shown in (15) and (16). The value of current angle which gives the highest value of torque is termed the maximum torque per amp (MTPA) angle. In the rotor geometry optimisation shown in [14] a fixed value is used throughout the optimisation procedure. However the optimal current angle will vary significantly as the geometries of the stator and rotor change. Therefore a method to obtain the MTPA angle with as small a number of simulations as possible was devised.

$$I_d = -\left(I_{prms}\sqrt{2}\right)\sin(\gamma) \tag{15}$$

$$I_q = \left(I_{prms}\sqrt{2}\right)\cos(\gamma) \tag{16}$$

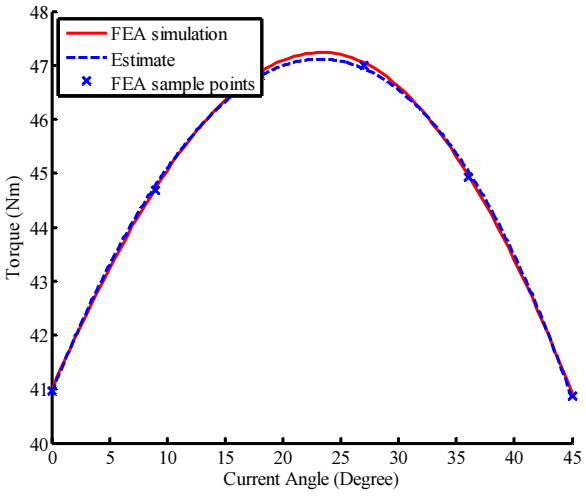

Fig. 4. Torque verus current angle, direct FE and estimated based on reduced number of FEAs

As the torque in a salient machine is a combination of synchronous and reluctance, it was found that a curve fit based

on two sinusoids (17) could be used to accurately describe the torque versus current angle characteristic (Fig. 4). It was found that six FE simulations were sufficient to obtain the coefficients of (17) with a high degree of certainty and good balance between accuracy and computational time.

$$T = a_1 \sin\big(b_1(\gamma + c_1)\big) + a_2 \sin(b_2(\gamma + c_2)) \qquad (17)$$

The full process is shown in Fig. 3. The MTPA is first calculated and with this the torque and inductance at the optimal current angle can then be deduced. To speed up computation, parallel computing of the separate FE simulations is used.

A particle swarm optimisation (PSO) is the chosen optimisation method. It is a robust stochastic evolutionary computation technique emulating the movement and intelligence of swarms. It has been shown to be effective in optimising difficult multidimensional discontinues problems, including electromagnetic design [15] and machine optimisation [16].

IV. Sensorless Capabillity Analysis

At each iteration of the optimisation process the inductance of the machine is determined. From this the saliency can be calculated simply:

$$Saliency = \frac{L_q}{L_d} \qquad (18)$$

It is desirable to estimate the sensorless control capability of a design at this operating point also. In particular the magnitude of the rotor position angular error due to cross coupling between the d and q axis inductances could be identified. FEA can be used to accomplish this.

It is not possible to simulate a voltage injection signal in a magneto-static FEA directly. Instead a high frequency current signal can be introduced on top of the fundamental value, and the high frequency flux linkage variation can be isolated to determine the sensorless capability of a machine design [10]. This can be demonstrated by substituting the voltage injection signal presented in (1), with current and transposing into the d and q axis reference (19), (20).

$$\begin{bmatrix} i_\alpha \\ i_\beta \end{bmatrix} = I_i \begin{bmatrix} -\sin(\theta_i) \\ cos(\theta_i) \end{bmatrix} \qquad (19)$$

$$\begin{bmatrix} i_d \\ i_q \end{bmatrix} = \begin{bmatrix} \cos(p\theta_r) & -\sin(p\theta_r) \\ sin(p\theta_r) & cos(p\theta_r) \end{bmatrix} \begin{bmatrix} i_\alpha \\ i_\beta \end{bmatrix} \qquad (20)$$

Where I_i is the magnitude of the injection current (which can be chosen arbitrarily), θ_i is the angle of the injection signal, θ_r is the position of the rotor and p is the number of pole pairs. If the rotor position is fixed, then an FE simulation can be calculated at several points along one full cycle of the injection signal (φ_{inj}). One additional simulation is performed with zero injection signal (φ_m), then the high frequency flux linkage (φ_{HF}) can be isolated as demonstrated in (21).

$$\varphi_{HF}(\theta_i)_{|\theta_r=const} = \varphi_{inj}(\theta_i)_{|\theta_r=const} - \varphi_{m_{|\theta_r=const}} \qquad (21)$$

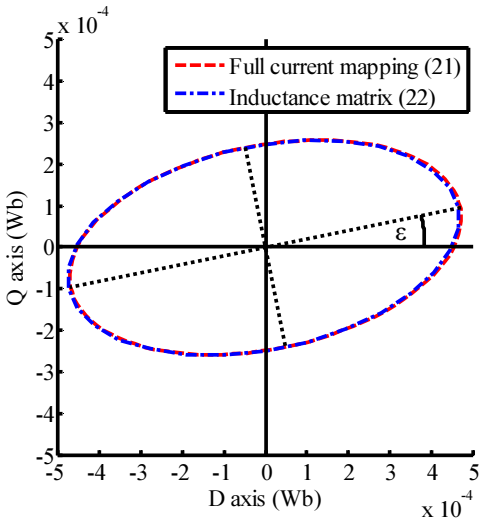

Fig. 5. Example high frequency flux linkage locus

Once isolated, the high frequency flux linkage variation can be plotted in the d and q axis domain to illustrate the saliency signature (Fig. 5). This is a plot at a fixed rotor position, over one full cycle of the injected signal. From this plot the sensorless capability of the machine can be deduced. If a magnetic saliency is present then the locus will form an elliptical shape. From this ellipse it is possible to identify the major and minor axes. The orientation of the major axis is the predicted rotor position of the sensorless algorithm. In Fig. 5 the correct rotor position is 0°, which corresponds to the x-axis, however the major axis is observed to be out of alignment. This rotation away from the correct rotor position is the sensorless angular error (ε) in electrical degrees.

The high frequency saliency calculated from the flux linkage locus in Fig. 5 will usually be greater in magnitude than the usual definition given by (18). This is due to the presence of cross-coupling between the d and q axis inductance. Attempting to maximise the high frequency saliency in the optimisation can result in a design with a high value of cross-coupling inductance, and a large angular error. Therefore the derivation of saliency given in (18) is used in the optimisation fitness function.

Employing multiple FE simulations to derive the high frequency flux linkage locus is not computationally feasible in an optimisation routine. However as demonstrated in [14], the flux linkage locus shown in Fig. 5 can be calculated with just three FE simulations, using the d, q and cross coupling inductance values defined in the previous section.

Considering the derivation of (3), only the inductance of the machine needs to be considered if the injection signal is a sufficiently high frequency relative to the rotational speed. The high frequency flux linkage can then be defined as:

$$\begin{bmatrix} \lambda_d \\ \lambda_q \end{bmatrix} = \begin{bmatrix} L_d & L_{dq} \\ L_{qd} & L_q \end{bmatrix} \begin{bmatrix} i_d(\theta_i) \\ i_q(\theta_i) \end{bmatrix} \qquad (22)$$

Using (21) the flux linkage locus can be computed rapidly with only three FE simulations. The resulting data is passed into a curve fitting algorithm which fits an ellipse to this data. With this the position and magnitude of the major and minor axes can

be determined, and the high frequency saliency and angular error calculated.

V. Fitness Function

With the value of torque, saliency and angular error calculated for a particular design, a fitness value is assigned to judge its suitability. A combined fitness value is used, which takes into account six separate criteria weighted in respect to their importance (23).

$$Fitness = \sum_{i=1}^{6} C_i F_i \tag{23}$$

The optimisation aims to maximise the value of fitness. Each fitness criteria (F_i) has a possible maximum value of one and a minimum value of zero. In the optimisation algorithm F_1 is torque, F_2 saliency, F_3 the winding current density, F_4 the angular error of the sensorless algorithm, F_5 the d-axis inductance and F_6 the cross sectional area of the PM. The form of each fitness value is shown below (24), with the exception of the sensorless error which is defined in (25). The target values for the fitness function are shown in Table IV.

$$F_i = \frac{abs(X_{target} - X_{PSO})}{X_{target}} \tag{24}$$

$$F_4 = 1 - \frac{Error_{PSO}}{45} \tag{25}$$

TABLE IV. Optimisation fitness function target values

Torque (Nm)	Saliency	Current Density (A/mm^2)	Ld (µH)	PM area (mm^2)
47	2	27	373	65

The fitness function is derived in this manner to ensure the design aims to meet the target value, but not exceed it. Values for the saliency and PM area are chosen so as to be challenging to meet. The error function is formulated to minimise the value of PM material used in order to realise a low cost design.

Table V shows a series of design outputs generated by the PSO optimisation given the same inputs and range of values within the optimisation. Each design was repeated 30 times and the best design included in the Table. Each optimal design of Table V differs in fitness function weights used. As can be seen there is much scope for varying the weightings for these performance criteria, and a multitude of designs can be produced.

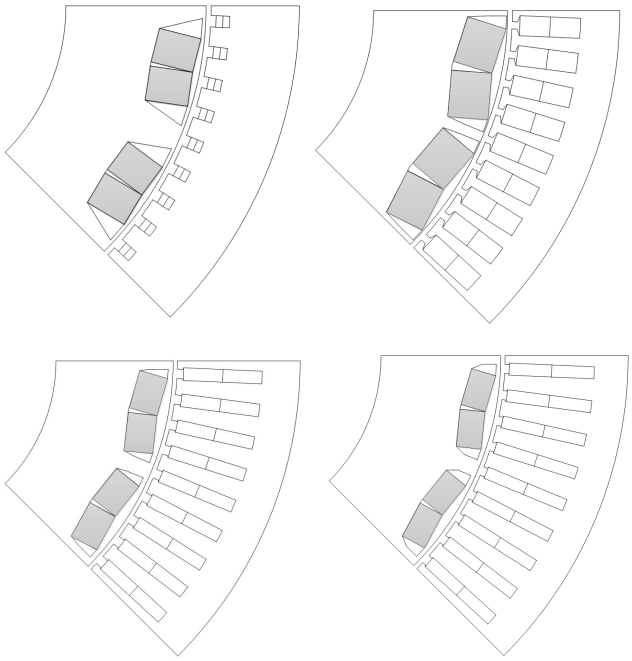

Fig. 6. Design 1 (top-left), 2 (top-right), 3 (bottom-left) and 4 (bottom-right) from table V

It is common in literature to optimise a sensorless oriented design based only on two criteria: torque and saliency. Design 1 in Table V and Fig. 6 demonstrate a result when equal weighting is given to both of these criteria and all other criteria removed (zero weighting). Without a target value for the winding current density the optimisation will minimise the winding window area to reduce saturation in the stator iron.

Design 2 in Table V additionally includes a weighting for the current density to force a more practical stator design. Through trial and error the weightings for these components can be adjusted to provide a satisfactory design. Highest priority is given to torque, as this is fundamental to meeting the specification. However it can be observed that the sensorless angular error is large. The optimisation has produced designs with high values of saliency, but no consideration to the cross coupling inductance. Design 3 addresses this by including a component in the fitness function for evaluating the angular error. The drawback is that a drop in the absolute value of the saliency has occurred.

Design 4 incorporates targets for the d-axis inductance and PM area. This is necessary to ensure the machine electrically meets the required operation envelope for the specification. In addition a significant saving in PM material can be gained with only a small reduction in performance.

TABLE V. Example design outputs with varying fitness function weightings

Design	Fitness Function Weighting Coefficients (C_i)						Results from optimisation					
	Torque (C_1)	*Saliency (C_2)*	*Current density (C_3)*	*Angular Error (C_4)*	*D-axis inductance (C_5)*	*PM Area (C_6)*	*Torque (Nm)*	*Saliency*	*Current Density (A/mm^2)*	*Angular Error (°)*	*D-axis inductance fitness*	*PM Area (mm^2)*
1	1.00	1.00	0.00	0.00	0.00	0.00	47.15	1.848	245.68	11.810	0.689	74.48
2	2.00	1.00	0.25	0.00	0.00	0.00	47.03	1.509	27.69	29.031	0.487	103.68
3	2.00	1.00	0.25	0.40	0.00	0.00	47.09	1.233	27.15	1.750	0.966	80.09
4	2.50	1.00	0.25	0.40	0.25	0.25	46.91	1.228	27.68	0.010	0.999	64.99

VI. FULL PERFORMANCE SIMULATION OF DESIGN 4

In order to constrain the number of computations the optimisation procedure considers a single fixed rotor position. However slotting effects are likely to affect both the torque and sensorless capability of the machine and therefore require investigation in the final selected design. Design 4 represented in Table V and Fig. 6 is selected to demonstrate a full simulation analysis.

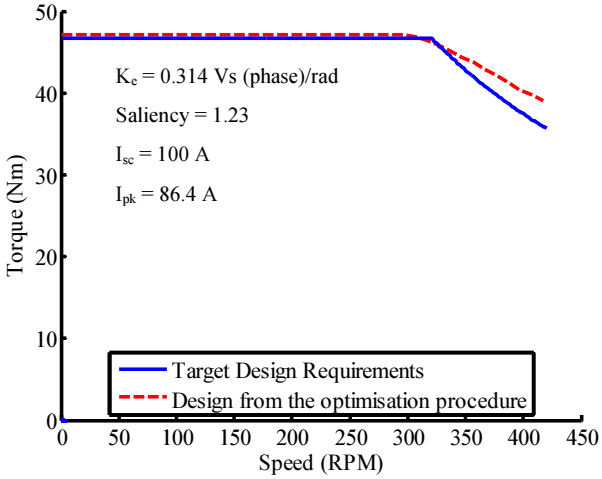

Fig. 7. Design 4 achieved operational envelope

Fig. 7 shows the calculated torque and speed performance. Included in Fig. 7 are the electrical parameters for this design. The parameters are close to those estimated in the initial design stage and therefore the machine closely matches the specification.

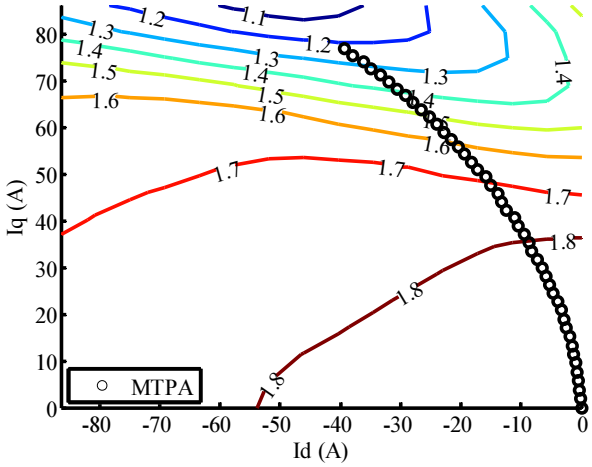

Fig. 8. Design 4 saliency contour plot

Fig. 8 presents a contour plot of the calculated saliency ratio. Included on the plot is the maximum torque per amp trajectory. This represents the optimum points at which the machine should be operated up to full rated current. This figure confirms the assumption that a machine designed only to rated current operation will maintain satisfactory saliency at lower loads.

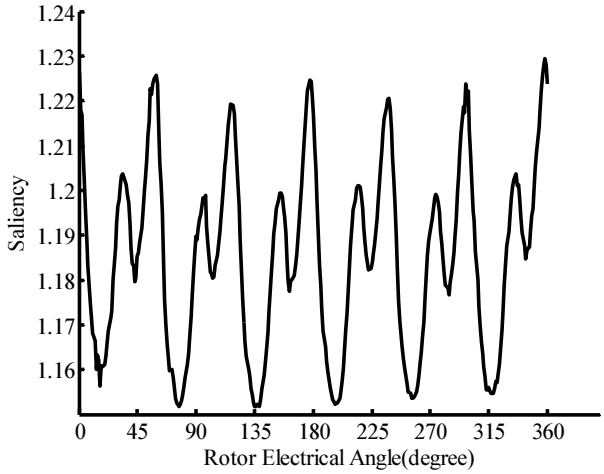

Fig. 9. Design 4 saliency variation with rotor position at rated current

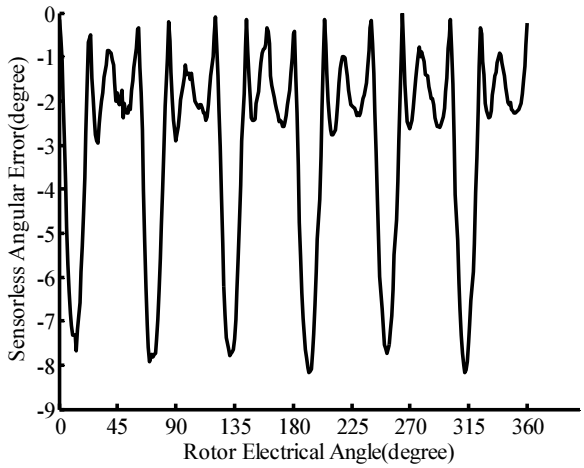

Fig. 10. Design 4 sensorless position error variation with rotor position at rated current

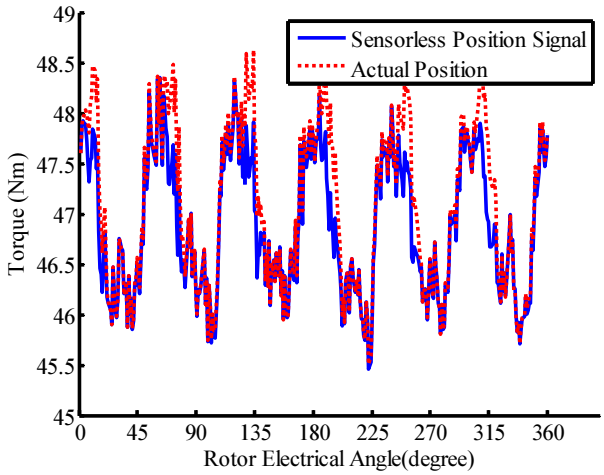

Fig. 11. Design 4 torque variation with rotor position utilising the sensorless predicted rotor position signal and accounting for cogging torque at rated current

Fig. 9 shows the saliency calculated at rated current over one full electrical cycle of the rotor. It demonstrates approximately a +/- 4% change in saliency with rotor position. Whilst this variation is not negligible the saliency ratio is seen to be above unity for all positions. Therefore in principal the rotor position should be detectable at all operating points and positions.

Fig. 10 demonstrates the variation of the sensorless angular error with rated current over one electrical cycle of the rotor and has a maximum of 8 degrees electrical. The effect of this error on torque production is estimated in Fig. 11. The expected sensorless rotor position is used to determine the phase current magnitudes, as it would be calculated in a machine drive. This is compared to a simulation where the exact rotor position is used. The angular error remains small enough to have little effect on the torque production.

VII. Conclusion

A design methodology for an IPM machine utilising a zero-speed injection based sensorless control has been presented. The focus of the research has been placed on developing a computationally efficient and accurate system that will optimise the parameters critical to the success of a zero speed sensorless algorithm, while meeting the requirements for the operation envelope and machine torque density.

The methodology contains two distinct stages to the design process. A trade study using analytical formulas allows a broad range of machine parameters to be investigated, critically the number of poles, slots and the resulting winding configuration. The second stage sizes the machine geometry using a combination of a particle swarm optimisation with a magneto-static FE solver.

A major benefit of the proposed approach is the optimisation considering the full machine, as both the stator and rotor are included in the electromagnetic design procedure. Building upon existing research in this field [14] a method to accurately predict the sensorless capability of a design with a small number of FE simulations is presented. The validity of this method is compared to a direct FE simulation showing excellent agreement.

A single objective optimisation is used with a combined fitness function made up of six separate components. The derivation and weightings for this function have been calibrated through numerous simulations. Through the use of several examples the derivation and effectiveness of this function is demonstrated.

A full FEA for the generated design is conducted. It is demonstrated that the machine design meets the required operational envelope. In addition the performance of the sensorless algorithm over one electrical cycle of the rotor is investigated. It can be concluded that the zero-speed sensorless algorithm will function at all operating points, and the performance degradation on torque at rated current due to cross-inductance is minimal. This demonstrates the accuracy and computational efficiency of the design methodology.

A prototype of a 16 pole, 72 slot, V-IPM machine is under construction to validate the proposed design methodology.

References

[1] R. Bojoi, M. Pastorelli, J. Bottomley, P. Giangrande, and C. Gerada, "Sensorless control of PM motor drives x2014; A technology status review," in *Electrical Machines Design Control and Diagnosis (WEMDCD), 2013 IEEE Workshop on*, 2013, pp. 168–182.

[2] A. S. Budden, R. Wrobel, D. Holliday, P. H. Mellor, A. Dinu, P. Sangha, and M. Holme, "Impact of Rotor Design on Sensorless Position Estimation," in *IEEE Industrial Electronics, IECON 2006 - 32nd Annual Conference on*, 2006, pp. 787–792.

[3] N. Bianchi and S. Bolognani, "Influence of rotor geometry of an interior PM motor on sensorless control feasibility," in *Industry Applications Conference, 2005. Fourtieth IAS Annual Meeting. Conference Record of the 2005*, 2005, vol. 4, p. 2553 – 2560 Vol. 4.

[4] Y. Kano, T. Kosaka, N. Matsui, and T. Nakanishi, "Design and experimental verification of a sensorless-oriented concentrated-winding IPMSM," in *Electrical Machines (ICEM), 2010 XIX International Conference on*, 2010, pp. 1–6.

[5] Y. Kano, T. Kosaka, N. Matsui, T. Takahashi, and M. Fujistuna, "Design of saliency-based sensorless drive IPM motors for hybrid electric vehicles," in *Energy Conversion Congress and Exposition (ECCE), 2012 IEEE*, 2012, pp. 4362–4369.

[6] N. Bianchi and S. Bolognani, "Influence of Rotor Geometry of an IPM Motor on Sensorless Control Feasibility," *Industry Applications, IEEE Transactions on*, vol. 43, pp. 87–96, 2007.

[7] N. Bianchi, S. Bolognani, J.-H. Jang, and S.-K. Sul, "Advantages of Inset PM Machines for Zero-Speed Sensorless Position Detection," *Industry Applications, IEEE Transactions on*, vol. 44, pp. 1190–1198, 2008.

[8] A. Faggion, E. Fornasiero, N. Bianchi, and S. Bolognani, "Sensorless Capability of Fractional-Slot Surface-Mounted PM Motors," *Industry Applications, IEEE Transactions on*, vol. 49, pp. 1325–1332, 2013.

[9] Y. Kano, T. Kosaka, N. Matsui, and M. Fujitsuna, "Sensorless-oriented design of concentrated-winding IPM motors for HEV drive application," in *Electrical Machines (ICEM), 2012 XXth International Conference on*, 2012, pp. 2709–2715.

[10] R. Wrobel, A. S. Budden, D. Salt, D. Holliday, P. H. Mellor, A. Dinu, P. Sangha, and M. Holme, "Rotor Design for Sensorless Position Estimation in Permanent-Magnet Machines," *Industrial Electronics, IEEE Transactions on*, vol. 58, pp. 3815–3824, 2011.

[11] D. Reigosa, K. Akatsu, N. Limsuwan, Y. Shibukawa, and R. D. Lorenz, "Self-sensing comparison of fractional slot pitch winding vs. distributed winding for FW- and FI-IPMSMs based on carrier signal injection at very low speed," in *Energy Conversion Congress and Exposition, 2009. ECCE 2009. IEEE*, 2009, pp. 3806–3813.

[12] R. Wrobel, A. S. Budded, D. Holliday, P. H. Mellor, and P. Sangha, "Design Considerations for Permanent Magnet Brushless Machines for Zero-Speed Sensorless Position Estimation," in *Industry Applications Conference, 2006. 41st IAS Annual Meeting. Conference Record of the 2006 IEEE*, 2006, vol. 3, pp. 1494–1500.

[13] N. Bianchi, D. Durello, and E. Fornasiero, "Multi-objective optimization of an Interior PM motor for a high-performance drive," in *Electrical Machines (ICEM), 2012 XXth International Conference on*, 2012, pp. 378–384.

[14] N. Bianchi, D. Durello, and E. Fornasiero, "Multi-objective optimization of a PM Assisted Synchronous Reluctance Machine, including torque and sensorless detection capability," in *Power Electronics, Machines and Drives (PEMD 2012), 6th IET International Conference on*, 2012, pp. 1–6.

[15] J. Robinson and Y. Rahmat-Samii, "Particle swarm optimization in electromagnetics," *Antennas and Propagation, IEEE Transactions on*, vol. 52, pp. 397–407, Feb. 2004.

[16] R. Wrobel and P. H. Mellor, "Particle Swarm Optimisation for the Design of Brushless Permanent Magnet Machines," in *Industry Applications Conference, 2006. 41st IAS Annual Meeting. Conference Record of the 2006 IEEE*, 2006, vol. 4, pp. 1891–1897.